PHYSICAL REVIEW B VOLUME 39, NUMBER 7 1 MARCH 1989

Multicritical points in the magnetic phase diagrams of axial and planar antiferromagnets

M. L. Plumer, A. Caillé, and Kevin Hood
Centre de Recherche en Physique du Solide et Département de Physique, Université de Sherbrooke, Sherbrooke, Québec, Canada J1K 2R1
(Received 9 May 1988)

The magnetic phase diagrams of weakly anisotropic axial and planar antiferromagnets with hexagonal crystal symmetry are studied using a Landau-type mean-field theory. Many novel types of multicritical points are predicted to occur as a result of competition between crystallographic and magnetic-field-induced anisotropies. These include bicritical, tricritical, tetracritical, and higher-order multicritical points, which can occur in a variety of combinations in the phase diagrams. The theory was shown previously to account for the observed magnetic phase diagram of $CsNiCl_3$ [Phys. Rev. Lett. **60**, 45 (1988)]. The results presented here may also be relevant for a number of related materials.

I. INTRODUCTION

The study of the behavior of weakly anisotropic antiferromagnets as a function of temperature and applied magnetic field has demonstrated a rich variety of phase-transition phenomena.[1] Much interest has been associated with the spin-flop transition which arises due to a competition between single-ion anisotropy and the anisotropy induced by the application of a magnetic field along the easy axis. This results in a magnetic phase diagram consisting of three regions: paramagnetic, antiferromagnetic, and spin-flopped phases. All three of these phases meet at a single point in the phase diagram, the so-called bicritical point, which represents the intersection of two lines of second-order transitions and one line of first-order transitions. Other types of multicritical points which have been studied include the tricritical point (at which a line of second-order transitions becomes a line of first-order transitions) as well as the tetracritical point (where four lines of second-order transitions meet). Only one of these types of multicritical points usually occurs for a given system. Multicritical points are of particular interest with regard to general descriptions of critical phenomena in terms of universality classes characterized by only the space dimensionality d and the number of components n of the order parameter. Crossover between different universality classes and the associated critical exponents have been much studied in systems which exhibit the kinds of multicritical points mentioned above.

In this work a previously developed nonlocal Landau free energy functional (Ref. 2, hereafter referred to as I) serves as a basis for a study of the magnetic phase diagrams of weakly anisotropic axial and planar antiferromagnets. The phenomenological model represents an expansion of the free energy up to fourth order in the spin density and is appropriate for the study of magnetic systems with hexagonal crystal symmetry in regions of the phase diagrams close to the paramagnetic state. Complicated phase diagrams are known to result from general analyses of Landau-type free energies of systems with multicomponent order parameters.[3] In addition to the usual diagrams with bicritical or tetracritical points, the model presented here gives rise to novel types of phase diagrams which include those with multicritical points where five lines of second-order phase transitions intersect and those which exhibit a coexistence of more than one type of multicritical point, when the magnetic field is directed parallel or perpendicular to the hexagonal c axis. Anisotropy terms of fourth order in the spin density are largely responsible for much of this rich behavior. In addition, the nature of the magnetic ordering in each region of the phase diagrams is described. Although the Landau treatment of phase transitions neglects critical fluctuations, it is known[1] that such mean-field theories account for all of the general features of magnetic phase diagrams.

The present study arose as an extension of our previous work using the Landau-type model (which did not include fourth-order anisotropy terms) to study the magnetic phase diagram of the axial antiferromagnet $CsNiCl_3$ (Ref. 4, hereafter referred to as II). This material has hexagonal crystal symmetry and exhibits an unusual type of multicritical point (with a magnetic field applied along the c axis) where three lines of second-order transitions and one line of first-order transitions meet. We show here that the addition of fourth-order anisotropy terms can lead to the stability of a new phase and that the phase coexistence point can become a higher-order multicritical point.

A class of hexagonal ABX_3 materials has attracted renewed interest recently because of their unusual quasi-one-dimensional magnetic properties at low temperatures (see, e.g., Refs. 5 and 6) and the rich variety of magnetic long-range order they show at lower temperatures (see, e.g., I and II and references therein). The principal objective of this work is to present a general study of the types of magnetic phase diagrams which result from an analysis of the Landau free energy which is applicable to a number of these systems (the phase diagram of $CsNiF_3$ was studied in I). Some controversy exists concerning the nature of the magnetically ordered phase of the axial anti-

ferromagnet $RbNiCl_3$. We propose two possible explanations of the observed magnetic phase diagram[7] which may aid in determining the real low-temperature magnetic state. Comments concerning the possible applications of some of the results to other ABX_3 materials, as well as to several rare-earth metals, are also made.

The remainder of this paper is organized as follows. In Sec. II the Landau free energy is presented, and some of its general properties are given. The phase diagrams for axial and planar antiferromagnets are presented in Secs. III and IV, respectively. Our conclusions and a discussion of the relevance of the results for $RbNiCl_3$ and some related materials are presented in Sec. V.

II. LANDAU FREE ENERGY

We consider systems which undergo a second-order phase transition (within mean-field theory) from the paramagnetic to a magnetically ordered state as the temperature is lowered. It is assumed that the magnetic ordering can be characterized by a single Fourier component of the spin density $\mathbf{s}(\mathbf{r})$ (in the absence of a magnetic field) so that

$$\mathbf{s}(\mathbf{r})=(V/N)\sum_{\mathbf{R}}\boldsymbol{\rho}(\mathbf{r})\delta(\mathbf{r}-\mathbf{R}) , \tag{1}$$

$$\boldsymbol{\rho}(\mathbf{r})=\mathbf{m}+\mathbf{S}e^{i\mathbf{Q}\cdot\mathbf{r}}+\mathbf{S}^*e^{-i\mathbf{Q}\cdot\mathbf{r}} , \tag{2}$$

where $\mathbf{R}$ gives the positions of the magnetic ions, $\mathbf{m}$ is the uniform magnetization induced by an applied field $\mathbf{H}$, and $\mathbf{S}$ and $\mathbf{Q}$ are the polarization and wave vectors, respectively, which characterize the long-range magnetic ordering. Using this expression for the spin density in the nonlocal Landau-type free energy developed in I for crystals with hexagonal symmetry (which includes terms up to fourth order in $\mathbf{s}$) leads to the free energy conveniently expressed as the sum of three terms

$$F=F_I+F_{A2}+F_{A4} , \tag{3}$$

where F_I includes all isotropic terms up to fourth order in $\mathbf{s}$, F_{A2} is the contribution from second-order anisotropy terms, and F_{A4} accounts for all fourth-order anisotropy terms. These three contributions to F are

$$F_I=A_QS^2+\tfrac{1}{2}A_0'm^2+B_1S^4+\tfrac{1}{2}B_2|\mathbf{S}\cdot\mathbf{S}|^2+\tfrac{1}{4}B_3m^4 +2B_4|\mathbf{m}\cdot\mathbf{S}|^2+B_5m^2S^2-\mathbf{m}\cdot\mathbf{H} , \tag{4}$$

$$F_{A2}=-A_z|S_z|^2-A_{z0}m_z^2 , \tag{5}$$

$$F_{A4}=\tfrac{1}{2}E_1(m_z^2|S_\perp|^2+m_\perp^2|S_z|^2)+E_2|S_z|^2|S_\perp|^2 +\tfrac{1}{4}E_3[S_z^2(S_x^{*2}+S_y^{*2})+\text{c.c.}]+\tfrac{1}{2}E_4m_z^2m_\perp^2 +\tfrac{3}{2}G_1|S_z|^4+3G_2m_z^2|S_z|^2+\tfrac{1}{4}G_3m_z^4 , \tag{6}$$

where $S^2=\mathbf{S}\cdot\mathbf{S}^*$, $\mathbf{S}_\perp=S_x\hat{\mathbf{x}}+S_y\hat{\mathbf{y}}$, and $\hat{\mathbf{z}}$ defines the direction of the hexagonal c axis. Temperature dependence enters in the usual way by assuming that the second-order isotropic coefficients can be expressed as

$$A_Q=a(T-T_Q),\quad A_0=a(T-T_0) , \tag{7}$$

where $A_0=A_0'-A_{z0}$ has been defined for convenience, $a>0$ and $T_Q>T_0$. In these expressions, T_Q is related to the magnetic ordering temperature and T_0 is related to the paramagnetic Curie temperature. Terms having the structure of the magnetic dipole-dipole interaction, which were shown in I to be responsible for the magnetically ordered state of $CsNiF_3$, are assumed here to be negligible for convenience and have been omitted from the free energy. Note that the free energy with fourth-order anisotropy set equal to zero, $\tilde{F}=F_I+F_{A2}$, is identical to the one used in II and is also consistent with tetragonal crystal symmetry.

In writing the free energy as given by (3)–(6) some assumptions regarding the wave vector $\mathbf{Q}$ have been made. Additional terms which contribute only if $2\mathbf{Q}=\mathbf{G}$, where $\mathbf{G}$ is a reciprocal lattice vector, were written explicitly (for convenience) in the corresponding free energy given in I. For this case, $\mathbf{S}$ may be chosen to be a real vector (see I) and the terms missing from (3)–(6) serve only to renormalize the existing terms. Thus, the free energy formulated here is appropriate for the case of $2\mathbf{Q}=\mathbf{G}$ if $\mathbf{S}$ is taken to be real. Other terms not included here contribute to the free energy only if $3\mathbf{Q}=\mathbf{G}$ or if $4\mathbf{Q}=\mathbf{G}$ (see Ref. 8 and I), and these cases will not be considered explicitly. For $CsNiCl_3$ and the other magnetic ABX_3 and rare-earth materials of interest here, the ordering wave vector satisfies the relation $6\mathbf{Q}=\mathbf{G}$ or is incommensurate with the lattice, and the free energy (3)–(6) is appropriate.

In a local formulation of the free energy, the relations $B_i=B_1$, $E_i=E_1$, and $G_i=G_1$ are satisfied. That these equalities are not in general true was shown in I (also see Ref. 8) to be a consequence of the wave-vector dependence of the kernels involved in the nonlocal formulation. Some of these relations are used here, however, in order to simplify the numerical calculations but these assumptions do not affect the qualitative results of interest.

An axial antiferromagnet is defined by $A_z>0$ (so that $\mathbf{S}\|\hat{\mathbf{z}}$ is the preferred configuration) and the planar case has $A_z<0$ (so that $\mathbf{S}\perp\hat{\mathbf{z}}$). The assumption of weak anisotropy implies, for example, that $|A_z|,|A_{z0}|\ll\Delta$, where

$$\Delta=A_0-A_Q=a(T_Q-T_0) \tag{8}$$

and $|E_i|,|G_i|\ll|B_i|$. These relations follow from the exchange-type origins of the isotropic terms in F_I which are assumed to be much stronger than the spin-orbit coupling (and other) effects which are responsible for the terms in F_{A2} and F_{A4}.

Interesting magnetic phase diagrams are a consequence of this model free energy as a result of competition between several important terms. The effect of the sign of the term in A_z has already been discussed. The term $B_2|\mathbf{S}\cdot\mathbf{S}|^2$ is minimized with a helical polarization if $B_2>0$ and with a linear polarization if $B_2<0$ (see Ref. 8). The term $2B_4|\mathbf{m}\cdot\mathbf{S}|^2$ is usually taken to be positive so that the configuration $\mathbf{S}\perp\mathbf{H}$ is preferred at high field values. For completeness, we also consider the resulting phase diagrams for $B_4<0$ so that $\mathbf{S}\|\mathbf{H}$ minimizes this term.

The polarization vector $\mathbf{S}$ is complex and in general has six degrees of freedom. We choose here to restrict somewhat the possible configurations of $\mathbf{S}$ by writing

$$\mathbf{S}=\mathbf{S}_1+i\mathbf{S}_2 , \tag{9}$$

where $\mathbf{S}_1$ and $\mathbf{S}_2$ are real vectors given by

$$\mathbf{S}_1=S\cos\beta(\sin\theta\hat{\boldsymbol{\rho}}_1+\cos\theta\hat{\mathbf{z}}) , \tag{10}$$

$$\mathbf{S}_2=S\sin\beta\hat{\boldsymbol{\rho}}_2 , \tag{11}$$

where $\hat{\boldsymbol{\rho}}_1\perp\hat{\boldsymbol{\rho}}_2\perp\hat{\mathbf{z}}$. In the following analysis we consider the two cases $\mathbf{H}\|\hat{\mathbf{z}}$ and $\mathbf{H}\|\hat{\boldsymbol{\rho}}_1$ and some motivation for the above choices for $\mathbf{S}_1$ and $\mathbf{S}_2$ is given in II. These expressions are flexible enough to encompass a wide variety of spin configurations, including linearly polarized states with $\mathbf{S}\|\hat{\boldsymbol{\rho}}_2$ and $\mathbf{S}\perp\hat{\boldsymbol{\rho}}_2$ as well as elliptically polarized states (including helical) with $\mathbf{S}\perp\hat{\mathbf{z}}$ and $\mathbf{S}\perp\hat{\boldsymbol{\rho}}_1$. Using (9)–(11) in (4)–(6) gives the following free energy appropriate for the study of magnetic phase diagrams with $\mathbf{H}\|\hat{\mathbf{z}}$ or $\mathbf{H}\|\hat{\boldsymbol{\rho}}_1$:

$$\begin{aligned}F=&A_Q S^2+\tfrac{1}{2}(A_0'-\delta A_{z0})m^2+\tfrac{1}{2}BS^4+(B_5+\tfrac{1}{2}\delta E_1)m^2S^2\\&+\tfrac{1}{4}(B_3+\delta G_3)m^4-mH+RS^2\cos^2\beta\cos^2\theta+PS^2\cos^2\beta\\&+2B_2S^4\cos^4\beta+E_3S^4\cos^4\beta\cos^2\theta\\&+\tfrac{1}{2}LS^4\cos^4\beta\cos^4\theta ,\end{aligned} \tag{12}$$

where

$$R=2B_4'(2\delta-1)m^2-A_z+\tfrac{1}{2}E_5S^2 , \tag{13}$$

$$P=2B_4(1-\delta)m^2-2B_2S^2 , \tag{14}$$

$$L=3G_1-2E_2-E_3 \tag{15}$$

with

$$B=2B_1+B_2,\quad B_4'=B_4-\tfrac{1}{4}E_1+\tfrac{3}{2}\delta G_2,\quad E_5=2E_2-E_3$$

and $\delta=1$ for $\mathbf{H}\|\hat{\mathbf{z}}$, $\delta=0$ for $\mathbf{H}\|\hat{\boldsymbol{\rho}}_1$. It has been assumed in writing (12) that $\mathbf{m}\|\mathbf{H}$ which is justified provided S^2 is not too large, i.e., for values of T and H close to the paramagnetic region of the phase diagram (see I).

The eight magnetically ordered phases which were found to minimize the free energy (12) are enumerated in Table I. In the cases of zero applied field or with $\mathbf{H}\|\hat{\mathbf{z}}$, phases 5 and 6 are degenerate in energy. This symmetry is broken by sixth-order planar anisotropy terms[9] which are not included in the present model. Expressions for β and θ appropriate for phases 3, 7, 8, and 9 (see Table I) are given by the following:

phase 3

$$\cos^2\beta=-(P+R)/(4\bar{B}_2S^2) , \tag{16}$$

where

$$\bar{B}_2=B_2+\tfrac{1}{2}E_3+\tfrac{1}{4}L ,$$

phase 7

$$\cos^2\beta=-P/(4B_2S^2) , \tag{17}$$

phase 8

$$\cos^2\beta=(RE_3-PL)/[(4B_2L-E_3^2)S^2] , \tag{18}$$

phase 8

$$\cos^2\theta=(PE_3-4RB_2)/(RE_3-PL) , \tag{19}$$

phase 9

$$\cos^2\theta=-(R+E_3S^2)/(LS^2) \tag{20}$$

with R, P, and L given by (13)–(15).

Consider now which of the phases enumerated in Table I can appear in the absence of an applied magnetic field. With the conditions that S is not too large and that anisotropy terms are small, the omission of fourth-order anisotropy terms does not affect the nature of these phases. F_{A4} is thus set equal to zero for the remainder of the analysis in this section for simplicity. We consider four cases depending on the signs of A_z and B_2. The notation of Table I will be used. The axial case of $A_z>0$ and $B_2>0$ has been considered by Zhu and Walker[9] and is reviewed in II. There are two phase transitions as the temperature is lowered. Phase 2 ($\beta=0$, $\theta=0$) exists in the interval $T_{N2}<T<T_{N1}$, where

$$T_{N1}=T_Q+A_z/a , \tag{21}$$

$$T_{N2}=T_{N1}-(A_z/a)(B/2B_2) , \tag{22}$$

and phase 3 exists at temperatures $T<T_{N2}$, where $\theta=0$ and β is given by (16) with $m=0$. It was shown in Ref. 9 that at sufficiently low temperatures, $\beta\to\pi/3$. This is valid provided the effects of fourth-order anisotropy terms are small. For the case $A_z>0$ and $B_2<0$, only the linearly polarized phase 2 is stable and there is a single phase transition at $T=T_{N1}$. For the planar case $A_z<0$ and $B_2>0$, only the helically polarized phase 4 exists as an ordered phase and there is a single phase transition at $T=T_Q$. For $A_z<0$ and $B_2<0$, there is a single phase transition to the linearly polarized phase 5 (or phase 6) at $T=T_Q$.

TABLE I. Ordered phases which minimize the free energy (12) where β and θ are defined by (9)–(11); L, E, and H denote linear, elliptical and helical polarizations, respectively; $0<\tilde{\theta}<\pi/2$ and $0<\tilde{\beta}<\pi/2$ as given by (16)–(20). Phase 1 is the paramagnetic state, $S=0$.

Phase	2	3	4	5	6	7	8	9
β	0	$\tilde{\beta}$	$\pi/4$	$\pi/2$	0	$\tilde{\beta}$	$\tilde{\beta}$	0
θ	0	0	$\pi/2$		$\pi/2$	$\pi/2$	$\tilde{\theta}$	$\tilde{\theta}$
Polarization	L	E	H	L	L	E	E	L
$\mathbf{S}$	$\|\hat{\mathbf{z}}$	$\perp\hat{\boldsymbol{\rho}}_1$	$\perp\hat{\mathbf{z}}$	$\|\hat{\boldsymbol{\rho}}_2$	$\|\hat{\boldsymbol{\rho}}_1$	$\perp\hat{\mathbf{z}}$		$\perp\hat{\boldsymbol{\rho}}_2$

III. PHASE DIAGRAMS FOR THE AXIAL ANTIFERROMAGNET

The equilibrium-state phases of the model free energy (12)–(15) are determined here for the case of $A_z > 0$ and with an applied magnetic field along the easy axis (Sec. III A) and also along the hard axis (Sec. III B). For each of these field directions, the four cases determined by the signs of B_2 and B_4 are considered separately. Many of the following results were determined by numerical minimization of the free energy with the local-formulation relations $B_1 = B_3 = B_5 > 0$ and $E_i = E_1 > 0$ assumed for simplicity. We denote the critical fields associated with the boundary between phases i and j by H_{ij} and the multicritical point indicated by the open circle in the phase diagrams is located at (T_m, H_m).

A. Field parallel to $\hat{z}$

1. $B_2 > 0$, $B_4 > 0$

This case was considered in II, with $F_{A4} = 0$, and applied to $CsNiCl_3$. Those results are reviewed here and the effects of adding fourth-order anisotropy terms are shown to give rise to additional novel types of multicritical points. This can be expected from a qualitative analysis of the terms in (12)–(15) which depend on θ. In the absence of fourth-order anisotropy, only terms proportional to $\cos^2\theta$ exist and, depending on the sign of the coefficient of this term, the free energy is minimized with either $\theta = 0$ or with $\theta = \pi/2$. This described the spin-flop transition discussed in II. An effect of fourth-order anisotropy is to add the term $\sim L \cos^4\theta$. This allows for the possibility that an intermediate phase with $0 < \theta < \pi/2$ minimizes the free energy provided that L is positive. It is shown below that existence of this intermediate phase 8 leads to interesting consequences for the structure of the magnetic phase diagram.

Figure 1 shows schematically the four types of phase diagrams found for the present case where first-order transition lines were determined numerically. It is straightforward to derive explicit expressions for second-order transition boundaries (given below); these results were also verified by direct numerical minimization of the free energy. Analytic expressions are also easy to determine for the multicritical points which involve the intersection of at least two lines of second-order transitions. Figure 1(a) corresponds to the type of phase diagram found if the parameter L were chosen to be less than some critical value L_{C1} (> 0) and is the type discussed in II (where in that work B_5 was chosen to be negative). Figures 1(b) and 1(c) correspond to increasing L and Fig. 1(d) is the type of diagram found if L is greater than some critical value L_{C2} ($L_{C2} > L_{C1}$). The principal effect of adding fourth-order anisotropy terms to the free energy is to stabilize phase 8 in a region of the phase diagram between phases 3 and 4. This leads to the appearance of a tricritical point in Figs. 1(b) and 1(c) and a new multicritical point (solid circle) in Fig. 1(c). The multicritical point shown by the open circle in Fig. 1(d) is of a novel type, representing the intersection of five lines of second-order transitions.

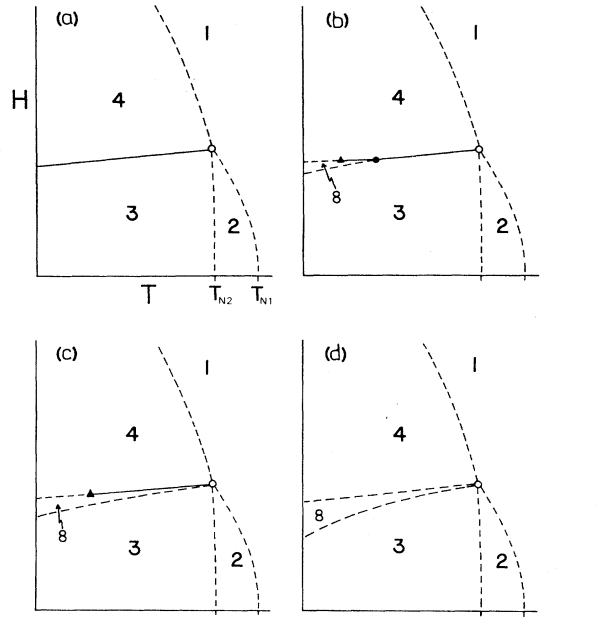

FIG. 1. Schematic phase diagrams for $\mathbf{H} \| \hat{z}$ and $A_z > 0$, $B_2 > 0$, $B_4 > 0$, where (a) $L < L_{C1}$, (b) and (c) $L_{C1} < L < L_{C2}$, (d) $L > L_{C2}$. Dashed lines denote second-order phase transitions and solid lines denote first-order phase transitions. Shown also are the multicritical point at (T_m, H_m) (open circle), tricritical point (triangle), and additional multicritical point (solid circle). Numbered phases are described in Table I.

The critical fields associated with the 1-2, 2-3, and 1-4 phase boundaries, as well as T_m and H_m, are not much affected by fourth-order anisotropy terms. These boundaries, with $E_i = 0$ and $G_i = 0$, are given by

$$H_{12}^z = (-A_1/B_6)^{1/2}[A_0 - (B_3/B_6)A_1] , \tag{23}$$

$$H_{23}^z = (A_2/B_7)^{1/2}[A_0 - 2(B_6/B)A_1 + (B_8/B_7)A_2] , \tag{24}$$

$$H_{14}^z = (-A_Q/B_5)^{1/2}[\Delta + (1 - B_3/B_5)A_Q] , \tag{25}$$

where

$$A_1 = a(T - T_{N1}), \quad A_2 = a(T - T_{N2}) \tag{26}$$

and

$$B_6 = B_5 + 2B_4, \quad B_7 = BB_4/B_2 - B_6, \quad B_8 = B_3 - 2B_6^2/B .$$

[Expressions (23) and (24) serve also to correct misprints that appear in Eqs. (15) and (16) in II.] The multicritical point is located at

$$T_m = T_{N1} - A_z B_6/(2aB_4) , \tag{27}$$

$$H_m = m_0[\Delta + (B_3 - B_5)m_0^2] , \tag{28}$$

where $m_0^2 = A_z/(2B_4)$. The exact expressions corresponding to (23)–(25), (27), and (28) with E_i and G_i included are found to be independent of the parameter L. Expressions for the second-order transition boundaries 3-8 and 4-8 are presented in Appendix A. Note that the

3-8 boundary is always a second-order transition and that H_{48}^z is independent of L.

Although it is not practicable to determine exact analytic expressions for the critical parameters L_{C1} and L_{C2}, some progress can be made to estimate these by comparing the critical field H_{38}^z and H_{48}^z. A necessary condition for the phase diagram of Fig. 1(d) to arise is $H_{48}^z > H_{38}^z$. By comparing the expressions for these critical fields given in Appendix A, this inequality is found to be approximately satisfied if $L > L_C$ with

$$L_C(T)=B_4[8A_z/\Delta+2a(E_2/B_1)(T-T_m)/\Delta] , \quad (29)$$

where $E_i \ll B_i$ and $A_z \ll \Delta$ have been used. This result serves as a crude guide to the stability of phase 8 when bounded by the two second-order phase transition lines. The fact that this critical value of L is dependent on temperature is partially responsible for the richness of the phase diagrams of Figs. 1(b) and 1(c). For $E_2 > 0$, $L_C(0) < L_C(T_m)$ and estimates of the critical parameters L_{C1} and L_{C2} are

$$L_{C1}=L_C(0)=L_{C2}-2B_4(E_2/B_1)T_m/(T_Q-T_0) , \quad (30)$$

$$L_{C2}=L_C(T_m)=8B_4A_z/\Delta . \quad (31)$$

These relations are reversed if $E_2 < 0$.

For quasi-one-dimensional magnetic materials one finds that $|T_0| \gg T_m, T_Q$. This leads to the conclusion that $L_{C1} \cong L_{C2}$ so that the phase diagrams of Figs. 1(b) and 1(c) result only for a very narrow range of parameter values. This has been verified numerically using parameter values based on those given for $CsNiCl_3$ in II. This result also implies that $H_{48}^z - H_{38}^z$ in Figs. 1(b) and 1(c) would be very small (100 G) for this class of materials.

2. $B_2 < 0$, $B_4 > 0$

For this case only linearly polarized states are stable and representative phase diagrams are shown in Fig. 2(a) for $L < L_{C1}$ and Fig. 2(b) for $L > L_{C2}$. The multicritical point in Fig. 2(a) is a bicritical point and in Fig. 2(b) is a tetracritical point. Both are located at (T_m, H_m) given by (27) and (28). Phase diagrams which also include a tricritical point and an additional multicritical point [of the types shown in Figs. 1(b) and 1(c)] result for intermediate values of L. The critical field H_{12}^z is given by (23) and $H_{15}^z = H_{16}^z = H_{14}^z$ given by (25). Expressions for the second-order transition phase boundaries 2-9 and 6-9 are given in Appendix B. Note that the 2-9 boundary is always a second-order phase transition and that H_{69}^z is independent of L. Estimates for the critical parameters L_{C1} and L_{C2} can be derived following the procedure outlined above by examining the condition $H_{69}^z > H_{29}^z$. This yields the result

$$L_{C1}=L_C(0)=L_{C2}-4B_4(E_6/B)T_m/(T_Q-T_0) , \quad (32)$$

where L_{C2} is given by (31) and $E_6 = E_2 + \frac{1}{2}E_3$ is assumed to be positive. Again, it is clear that $L_{C1} \cong L_{C2}$ if $|T_0| \gg T_Q, T_m$.

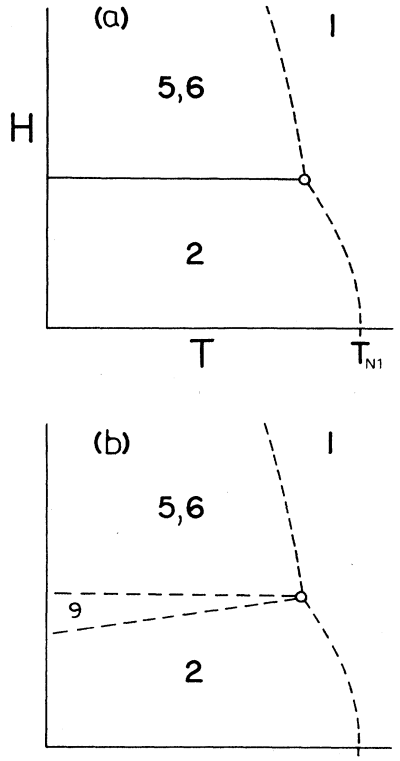

FIG. 2. Schematic phase diagrams for the both cases of $\mathbf{H}\|\hat{\mathbf{z}}$, $A_z > 0$, $B_2 < 0$, $B_4 > 0$ and $\mathbf{H}\|\hat{\boldsymbol{\rho}}_1$, $A_z > 0$, $B_2 < 0$, $B_4 < 0$, where (a) $L < L_{C1}$ and (b) $L > L_{C2}$. For $\mathbf{H}\|\hat{\mathbf{z}}$, phase 5 is degenerate with phase 6.

3. $B_2 > 0$, $B_4 < 0$

With B_4 negative, a magnetic field serves to stabilize the configuration $\mathbf{S}\|\mathbf{H}$ so that phase 2 exists as an equilibrium high-field state and the resulting phase diagram is shown in Fig. 3. This type of diagram also arises for the case of $B_4 > 0$ with $\mathbf{H}\|\hat{\boldsymbol{\rho}}_1$ as discussed below and in II. The critical fields for the 1-2 and 2-3 phase boundaries are given by (23) and (24), respectively.

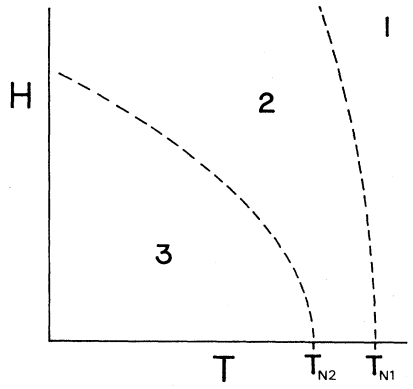

FIG. 3. Schematic phase diagram for the both cases of $\mathbf{H}\|\hat{\mathbf{z}}$, $A_z > 0$, $B_2 > 0$, $B_4 < 0$ and $\mathbf{H}\|\hat{\boldsymbol{\rho}}_1$, $A_z > 0$, $B_2 > 0$, $B_4 > 0$.

4. $B_2<0$, $B_4<0$

Only phase 2 exists as an ordered state, and the 1-2 boundary is given by the critical field (23).

B. Field parallel to $\hat{\rho}_1$

1. $B_2>0$, $B_4>0$

The phase diagram for this case was considered in II and is the same as for the case of $\mathbf{H}\|\hat{\mathbf{z}}$, $B_2>0$, $B_4<0$ discussed above and illustrated in Fig. 3. The appropriate critical fields, with $E_i=G_i=0$, are

$$H_{12}^{\rho}=(-A_1/B_5)^{1/2}[\Delta'+A_z+(1-B_3/B_5)A_1] \quad (33)$$

$$H_{23}^{\rho}=(-A_2/B_5)^{1/2}[\Delta'+A_Q+(B_5/B_2)A_z -(B_3/B_5)A_2]\,, \quad (34)$$

where $\Delta'=\Delta+A_{z0}$. The corresponding phase diagram in II shows these critical fields increasing with temperature since $B_5<0$ in that work.

2. $B_2<0$, $B_4>0$

Since the applied field is perpendicular to $\mathbf{S}$, and B_4 is positive, the zero-field phase 2 state remains stable at high fields. No other states exist in the phase diagram, which corresponds to the case of $\mathbf{H}\|\hat{\mathbf{z}}$, $B_2<0$, $B_4<0$ discussed above. The 1-2 phase boundary is given by the critical field H_{12}^{ρ} (33).

3. $B_2>0$, $B_4<0$

This combination of signs for B_2 and B_4 produces a very complicated phase diagram with $\mathbf{H}\|\rho_1$ due to the fact that $B_2>0$ stabilizes helically polarized structures whereas $B_4<0$ stabilizes linear polarization. The resulting phase diagrams for the two cases of small L (>0) and larger L are shown in Figs. 4(a) and 4(b), respectively. For intermediate values of L (not shown), tricritical and additional multicritical points can be present as is easily imagined in view of the results shown in Fig. 1.

The bicritical point in Fig. 4(a) and the tetracritical point in Fig. 4(b) are both located at (T_m,H_m) given (with $E_i=G_i=0$) by

$$T_m=T_{N1}+A_zB_5/(2aB_4)\,, \quad (35)$$

$$H_m=m_0[\Delta'+A_z+(B_3-B_5)m_0^2]\,, \quad (36)$$

where $m_0^2=-A_z/(2B_4)$. Referring to Fig. 4(b), the multicritical point at the intersection of the phases 6, 7, 8, and 9 occurs (again, with $E_i=G_i=0$) at

$$T_{6789}=T_m-A_zB/(2aB_2)\,, \quad (37)$$

$$H_{6789}=H_m+m_0A_z(B_6-\tfrac{1}{2}B)/B_2 \quad (38)$$

and the multicritical point at the intersection of phases 2, 3, 8, and 9 occurs at

$$T_{2389}=T_m-A_zB/(2aB_2)\,, \quad (39)$$

$$H_{2389}=H_m+m_0A_z(B_5-\tfrac{1}{2}B)/B_2\,. \quad (40)$$

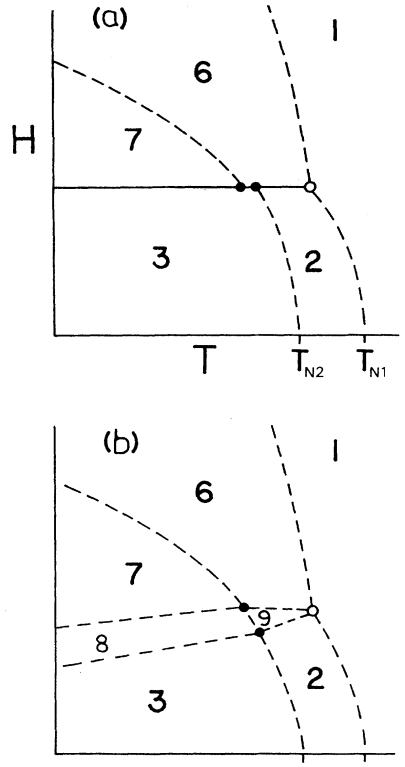

FIG. 4. Schematic phase diagrams for $\mathbf{H}\|\hat{\rho}_1$, $A_z>0$, $B_2>0$, $B_4<0$, where (a) $L<L_{C1}$ and (b) $L>L_{C2}$.

The 1-2 and 2-3 phase boundaries are given by the expressions (33) and (34), respectively. The critical field corresponding to the 1-6 boundary can be expressed as

$$H_{16}^{\rho}=(-A_Q/B_6)^{1/2}[\Delta'+(1-B_3/B_6)A_Q] \quad (41)$$

and the 6-7 boundary is given (with $E_i=G_i=0$) by

$$H_{67}^{\rho}=(-A_Q/B_9)^{1/2}[\Delta'+(1-B_{10}/B_9)A_Q]\,, \quad (42)$$

where

$$B_9=B_6'-2B_1B_4/B_2,\quad B_{10}=B_3-2B_4^2/B_2-2B_4B_6'/B_2\,,$$

$$B_6'=B_4+B_5\,.$$

Exact expressions for the critical fields H_{29}^{ρ} and H_{69}^{ρ} are given in Appendix C and for H_{38}^{ρ} and H_{78}^{ρ} in Appendix D. An expression for the critical field H_{89}^{ρ} is straightforward to derive but is not given here as it represents only a very small line in the phase diagram and is complicated to express.

4. $B_2<0$, $B_4<0$

The phase diagram for this case is as shown in Fig. 2. The corresponding critical fields are given by (33), (41), and in Appendix C.

IV. PHASE DIAGRAMS FOR THE PLANAR ANTIFERROMAGNET

The magnetic phase diagrams are determined here for the case of $A_z<0$ with an applied magnetic field along

the easy axis (Sec. IV A) and also along the hard axis (Sec. IV B). Again, for each of these field directions, the four cases determined by the signs of B_2 and B_4 were considered separately and the local-formulation relations $B_1=B_3=B_5>0$ and $E_1=E_1>0$ were assumed for simplicity for the numerical analysis.

A. Field parallel to $\hat{\rho}_1$

1. $B_2>0$, $B_4>0$

The phase diagrams for this case is shown in Fig. 5 and exhibits several interesting features. The application of a magnetic field is seen to break the symmetry of the helical state at the Néel temperature T_Q in favor of the linearly polarized phase[10] 5. This arises because it is terms of order S^2 which determine the first-ordered phase that appears as the temperature is lowered. The term $B_2|\mathbf{S}\cdot\mathbf{S}|^2$ which is responsible for the stabilization of the zero-field helical polarization is proportional to S^4 whereas the term $B_4|\mathbf{m}\cdot\mathbf{S}|^2$ favors the linear configuration and is quadratic in S. Figures 5(a)–5(d) represent the results obtained for increasing L, where again we define L_{C1} and L_{C2} such that $L<L_{C1}$ corresponds to Fig. 5(a) and $L>L_{C2}$ corresponds to Fig. 5(d). The structure of the phase diagrams at intermediate values of L is of a different character from that seen in Fig. 1, but again these diagrams exhibit a tricritical point and an additional multicritical point (denoted by the solid circle). The open circle in Fig. 5(a) represents a bicritical point and in Fig. 5(d) it is a tetracritical point.

The critical fields corresponding to the second-order phase transitions in Fig. 5 are (with $E_i=G_i=0$)

$$H_{15}^{\rho}=(-A_Q/B_5)^{1/2}[\Delta'+(1-B_3/B_5)A_Q]\ , \tag{43}$$

$$H_{57}^{\rho}=(-A_Q/B_{12})^{1/2}[\Delta'+(1-B_{13}/B_{12})A_Q]\ , \tag{44}$$

$$H_{35}^{\rho}=(-A_3/B_5)^{1/2}[\Delta'+A_z(\tfrac{1}{2}BB_3/B_5-B_5)/B_2+(1-B_3/B_5)A_Q]\ , \tag{45}$$

where

$$B_{12}=BB_4/B_2+B_5,\quad B_{13}=B_3+2B_4B_5/B_2\ ,$$

and $A_3=A_Q-\frac{1}{2}A_zB/B_2$. Expressions for H_{38}^{ρ} and H_{78}^{ρ} are given in Appendix D. The multicritical point denoted by the open circles in Fig. 5 is at (T_m,H_m) given by

$$T_m=T_Q-\tfrac{1}{2}|A_z|B_{12}/(aB_4)\ , \tag{46}$$

$$H_m=m_0[\Delta'+(B_{13}-B_{12})m_0^2]\ , \tag{47}$$

where $m_0^2=|A_z|/(2B_4)$. Estimates for the critical parameters L_{C1} and L_{C2} can be made as before by analyzing the condition $H_{38}^{\rho}>H_{78}^{\rho}$ with the results

$$L_{C1}=L_C(T_m)=8B_4|A_z|/\Delta\ , \tag{48}$$

$$L_{C2}=L_C(0)=L_{C1}+2B_4(E_2/B_1)T_m/(T_Q-T_0)\ . \tag{49}$$

Note that these expressions are the reverse of the results (30) and (31), which is responsible for the phase diagrams at intermediate values of L in Fig. 5 having a structure different from the corresponding phase diagrams in Fig. 1.

2. $B_2<0$, $B_4>0$

Only the linearly polarized phase 5 exists as an ordered state (degenerate with phase 6 at $H=0$), and the 1-5 phase boundary is given by (43).

3. $B_2>0$, $B_4<0$

The linearly polarized phase ($\mathbf{S}\|\mathbf{H}$) is stabilized here at high fields and the resulting phase diagram is shown in Fig. 6. Note the symmetry breaking at the Néel tempera-

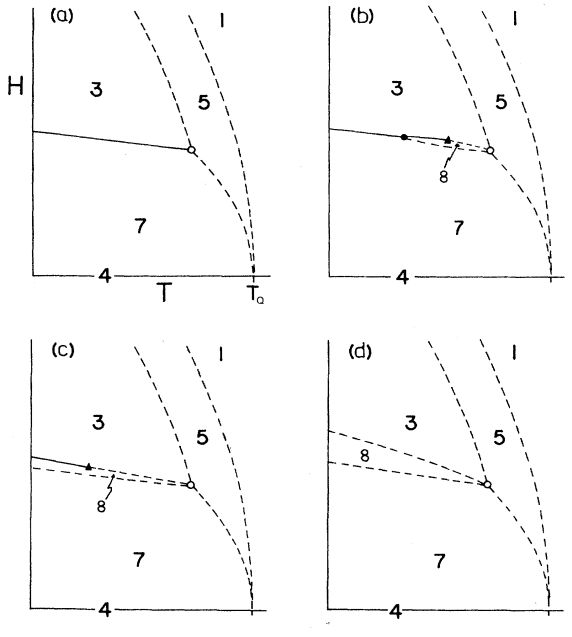

FIG. 5. Schematic phase diagrams for $\mathbf{H}\|\hat{\rho}_1$ and $A_z<0$, $B_2>0$, $B_4>0$, where (a) $L<L_{C1}$, (b) and (c) $L_{C1}<L<L_{C2}$, (d) $L>L_{C2}$ (otherwise, as in Fig. 1).

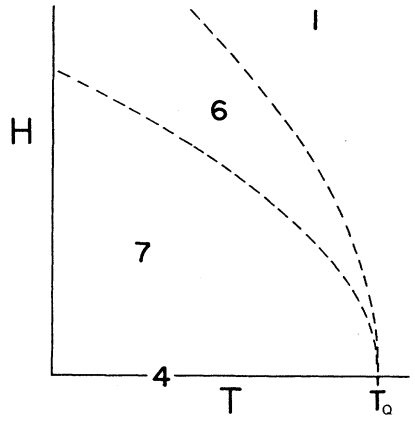

FIG. 6. Schematic phase diagram for the cases of $\mathbf{H}\|\hat{\rho}_1$, $A_z<0$, $B_2>0$, $B_4<0$.

ture with the application of a field. The 1-6 and 6-7 phase boundaries are expressed by (41) and (42), respectively.

4. $B_2 < 0$, $B_4 < 0$

For this case, only phase 6 exists as an ordered state (degenerate with phase 5 at $H=0$) with H_{16}^{ρ} given by (41).

B. Field parallel to $\hat{z}$

1. $B_2 > 0$, $B_4 > 0$

Here, the zero-field phase 4 is also stable at $H \neq 0$ and is the only ordered state which occurs. The 1-4 boundary is given by the expression (25).

2. $B_2 < 0$, $B_4 > 0$

Only the energetically degenerate phases 5 or 6 appear in the phase diagram with $H_{15}^{z} = H_{16}^{z} = H_{14}^{z}$ as given by (25).

3. $B_2 > 0$, $B_4 < 0$

The phase diagram for this case is shown in Fig. 7. The low- and high-field regions are similar to the high- and low-field regions, respectively, of the phase diagrams in Fig. 1. This feature arises because at high-field values the term $B_4|\mathbf{m}\cdot\mathbf{S}|^2$ acts as an effective uniaxial anisotropy if B_4 is negative and effective planar anisotropy if B_4 is positive. Figures 7(a) and 7(b) correspond, again, to $L < L_{C1}$ and $L > L_{C2}$, respectively, with intermediate values of L yielding phase diagrams with structure as shown in Figs. 5(b) and 5(c). This follows from an analysis of the condition $H_{38}^{z} > H_{48}^{z}$ (using results given in Appendix A), as before, and leads to the results (48) and (49), with $B_4 \rightarrow |B_4|$. The critical fields and location of the multicritical point denoted by the open circles in Fig. 7 are the same as for Fig. 1.

4. $B_2 < 0$, $B_4 < 0$

Figure 8 shows the phase diagram for this case for small and large values of L. The results indicate that, as with the previous case, there is a high-field–low-field symmetry with the corresponding results for the axial antiferromagnet shown in Fig. 2. Note again that phases 5 and 6 are degenerate for a field applied along the $\hat{z}$ axis. An analysis of the condition $H_{29}^{z} > H_{59}^{z}$ (or H_{69}^{z}) shows that for intermediate values of L the same structure of tricritical and additional multicritical point occurs as depicted in Fig. 5. The phase boundaries and location of the multicritical point denoted by the open circle are given by the same expressions as for Fig. 2.

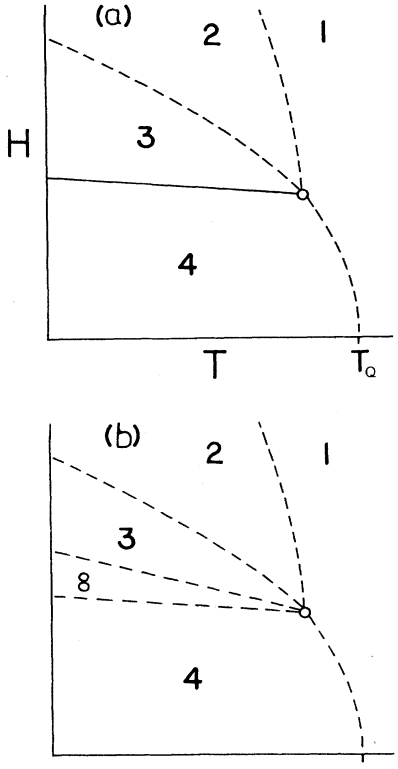

FIG. 7. Schematic phase diagrams for $\mathbf{H}\|\hat{z}$, $A_z < 0$, $B_2 > 0$, $B_4 < 0$, where (a) $L < L_{C1}$ and (b) $L > L_{C2}$.

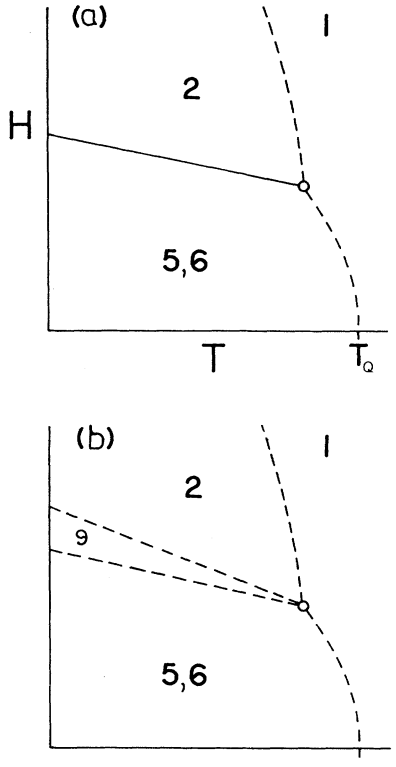

FIG. 8. Schematic phase diagrams for $\mathbf{H}\|\hat{z}$, $A_z < 0$, $B_2 < 0$, $B_4 < 0$, where (a) $L < L_{C1}$ and (b) $L > L_{C2}$.

V. DISCUSSION AND CONCLUSIONS

The analysis of the Landau-type free energy presented in this work has demonstrated that the magnetic phase diagrams of axial and planar antiferromagnets can exhibit a rich variety of multicritical point phenomena. Much of the complicated structure was shown to be a consequence of fourth-order anisotropy terms included in the free energy for the study of crystals with hexagonal symmetry. A principal effect of these terms is to stabilize an intermediate state at the spin-flop phase boundary. This leads to the appearance of up to three different types of multicritical points on a single phase diagram [see Figs. 1(b) and 5(b)], although such configurations are expected to exist for only a narrow range of parameter values for many materials. A novel type of multicritical point where five lines of second-order transitions meet was also shown to be a consequence of the model with sufficiently strong fourth-order anisotropy [see Figs. 1(d) and 7(b)]. Phase diagrams with interesting structures were found even in the absence of fourth-order anisotropy effects [see Figs. 1(a), 2(a), 4(a), 5(a), 7(a), and 8(a)]; these results also apply to crystals with tetragonal crystal symmetry.

Multicritical points which represent the intersection of more than three phases are unusual in the two-dimensional space of physically accessible thermodynamic fields H and T. That this is possible was shown by Gufan and Sakhnenko[11] for a multicomponent order parameter with the number of components larger than or equal to three, provided that some of the phases are separated by second-order transitions. This is not a violation of the Gibbs phase rule (which applies to first-order transitions) due to the fact that the thermodynamic potentials of the different phases in equilibrium are extrema of the same free energy for the case of second-order phase transitions. A proper classification of the multicritical points of our model would require an analysis of the phase diagrams in a five-dimensional thermodynamic field space, three of which being the physically inaccessible symmetry breaking fields conjugate with the three components of the order parameter $\mathbf{S}$ [see (9)–(11)]. The general topology[12] and dimensions of the hypersurfaces of critical points associated with the phase diagram for $CsNiCl_3$ are under study and will be published elsewhere.

The theoretical study in Ref. 4 was motivated by the experimentally determined magnetic phase diagram of $CsNiCl_3$ based on the susceptibility data of Johnson, Rayne, and Friedberg.[7] Experimental data for the magnetic phase diagram of isomorphic $RbNiCl_3$ with $\mathbf{H}\|\hat{\mathbf{z}}$ (showing a spin-flop transition) are also presented in that work and we attempt here to explain these results with our model. $RbNiCl_3$ appears to exhibit a single phase transition at $T_N \cong 11.2$ K. The first neutron diffraction study[13] indicated that the ordered structure corresponds to phase 3; a second study[14] suggested the structure is that of phase 2; a third work[15] corroborated the results of the first study. Recent specific-heat measurements[16] show a single anomaly at $T \cong 11.0$ K.

The two results for $RbNiCl_3$ that there is only a single phase transition and that the ordered state is phase 3 are not consistent with hexagonal crystal symmetry and mean-field theory. The ordered phase which first appears as the temperature is lowered has the direction of the associated polarization vector $\mathbf{S}$ determined by second-order anisotropy terms. In this case, there is only the term $-A_z|S_z|^2$ so that either $\mathbf{S}\|\hat{\mathbf{z}}$ or $\mathbf{S}\perp\hat{\mathbf{z}}$, in contrast with the configuration of $\mathbf{S}$ or phase 3. Phase 3 can exist only if the intermediate phase 2 is present, as is the case with $CsNiCl_3$ and as is believed to describe $CsNiBr_3$, $CsMnI_3$, $RbNiBr_3$, VCl_2, and Er (see Refs. 17–21). Our model is, however, consistent with phase 2 being the only ordered state and there being a single phase transition if $B_2 < 0$. The schematic phase diagram of Fig. 2(a) is in qualitative agreement with the experimental results of Ref. 7. An alternative explanation of experimental results is that phase 3 exists at low temperature but phase 2 is also present as an intermediate state as in the case of $CsNiCl_3$. This proposal is based on the possibility that $T_{N1} - T_{N2}$ is sufficiently small that the existence of two distinct phase transitions has thus far been undetected. The schematic phase diagram for this case ($B_2 > 0$) is shown in Fig. 1(a). Further experimental work is desirable to determine if one of the above explanations is correct.

Detailed experimental results on the behavior of the magnetically ordered phases near the Néel temperature in the presence of an applied magnetic field are scarce in related materials. Phase 4 describes the zero-field ordered state of the planar antiferromagnets $CsMnBr_3$ and Ho. These materials have recently been shown[22,23] to exhibit anomalous behavior suggesting a splitting of the Néel temperature with the application of a field in the basal plane, as shown schematically in Figs. 5 and 6. The class of related materials[24,25] $RbVX_3$ and $CsVX_3$ (X = Cl, Br, I) also deserve further study to determine the structure of their associated phase diagrams. The axial antiferromagnets mentioned above which show successive zero-field magnetic phase transitions similar to $CsNiCl_3$ can be expected to exhibit interesting field-induced phases as well. A spin-flop transition induced by a field applied along the c axis has been observed[28] in $CsMnI_3$.

As mentioned in the Introduction, crossover behavior associated with multicritical phenomena is of interest and the novel types of phase coexistence points described by our mean-field model provides a basis for further theoretical study.

ACKNOWLEDGMENTS

Research supported by Natural Sciences and Engineering Research Council (NSERC) of Canada and Fonds pour la Formation de Chercheurs et l'Aide à la Recherche (FCAR) du Québec. One of us (K.H.) acknowledges additional support from NSERC.

APPENDIX A

With the magnetic field $\mathbf{H}\|\hat{\mathbf{z}}$, the second-order transition 3-8 phase boundary can be expressed as

$$H_{38}^{z} = m[\tilde{A}_0 - 2(\tilde{B}_5/\tilde{B})\tilde{A}_Q + (\tilde{B}_3 - 2\tilde{B}_5^2/\tilde{B})m^2], \quad \text{(A1)}$$

$$m^2 = [A_z\tilde{B}(4B_2 + E_3) + \tilde{A}_Q W]/[2B_4'\tilde{B}(4B_2 + E_3) - \tilde{B}_5 W] \quad \text{(A2)}$$

with

$$W=2B_2(L+2E_3)+\tfrac{1}{2}E_3E_5 , \tag{A3}$$

$$\tilde{A}_0=A_0+4A_zB_4'/4\bar{B}_2 , \tag{A4}$$

$$\tilde{A}_Q=A_Q-2A_zB_2'/4\bar{B}_2 , \tag{A5}$$

$$\tilde{B}=B-4(B_2')^2/4\bar{B}_2 , \tag{A6}$$

$$\tilde{B}_3=\bar{B}_3-8(B_4')^2/4\bar{B}_2 , \tag{A7}$$

$$\tilde{B}_5=\bar{B}_5+4B_2'B_4'/4\bar{B}_2 , \tag{A8}$$

and

$$B_2'=B_2-\tfrac{1}{2}E_5,\quad \bar{B}_3=B_3+G_3 ,$$

$$\bar{B}_5=B_5+\tfrac{1}{2}E_1,\quad \bar{B}_2=B_2+\tfrac{1}{2}E_3+\tfrac{1}{4}L .$$

The 4-8 phase boundary is given by

$$H_{48}^z=m[A_0-(\bar{B}_5/B_1)A_Q+(\bar{B}_3-\bar{B}_5^2/B_1)m^2] , \tag{A9}$$

$$m^2=(A_z+\tfrac{1}{2}A_QE_2/B_1)/(2B_4'-\tfrac{1}{2}\bar{B}_5E_2/B_1) . \tag{A10}$$

APPENDIX B

With the magnetic field $\mathbf{H}\|\hat{\mathbf{z}}$, the second-order transition 2-9 boundary can be written as

$$H_{29}^z=m[A_0+2(B_6/L')A_z+(\bar{B}_3-4B_4'B_6/L')m^2] , \tag{B1}$$

$$m^2=(A_zB'+A_1L')/(2B_4'B'-B_6L') , \tag{B2}$$

where

$$B'=B+L+2E_6,\quad L'=L+E_6,\ \text{and}\ E_6=E_2+\tfrac{1}{2}E_3 .$$

The 6-9 phase boundary is given by

$$H_{69}^z=m[A_0+2(\bar{B}_5/E_6)A_z+(\bar{B}_3-4B_4'\bar{B}_5/E_6)m^2] , \tag{B3}$$

$$m^2=(A_zB+A_QE_6)/(2B_4'B-\bar{B}_5E_6) . \tag{B4}$$

APPENDIX C

With the magnetic field $\mathbf{H}\|\hat{\boldsymbol{\rho}}_1$, the second-order transition 2-9 phase boundary can be written as

$$H_{29}^{\rho}=m[A_0'+2A_z\bar{B}_5/L'+(B_3+4B_4'\bar{B}_5/L')m^2] , \tag{C1}$$

$$m^2=-(A_zB'+A_1L')/(2B_4'B'+L'\bar{B}_5) , \tag{C2}$$

where $\bar{B}_5$, B', and L' are defined in Appendixes A and B, and the 6-9 phase boundary is given by

$$H_{69}^{\rho}=m[A_0'+2A_zB_6/E_6+(B_3+4B_4'B_6/E_6)m^2] , \tag{C3}$$

$$m^2=-(A_zB+A_QE_6)/(2B_4'B+E_6B_6) , \tag{C4}$$

where $E_6=E_2+\frac{1}{2}E_3$.

APPENDIX D

With the magnetic field $\mathbf{H}\|\hat{\boldsymbol{\rho}}_1$, the second-order transition 3-8 phase boundary can be written as

$$H_{38}^{\rho}=m[a_0-2(b_5/\tilde{B})\tilde{A}_Q+(b_3-2b_5^2/\tilde{B})m^2] , \tag{D1}$$

$$m^2=\frac{-\{A_z\tilde{B}(4B_2+E_3)+\tilde{A}_QW\}}{\{\tilde{B}[8B_4\bar{B}_2-\frac{1}{2}E_1(4B_2+E_3)]+b_5W\}} , \tag{D2}$$

where $\tilde{A}_Q$, $\tilde{B}$, and W are defined in Appendix A and

$$a_0=A_0'+A_zE_1/(4\bar{B}_2) , \tag{D3}$$

$$b_3=B_3-\tfrac{1}{2}E_1^2/(4\bar{B}_2) , \tag{D4}$$

$$b_5=B_5+B_2'E_1/(4\bar{B}_2) . \tag{D5}$$

The 7-8 phase boundary is given by

$$H_{78}^{\rho}=m[A_0'-A_Q(B_4+B_5)/B_1+B_{11}m^2] , \tag{D6}$$

$$m^2=\frac{-[A_z+A_QE_2/(2B_1)]}{[B_4'+\frac{1}{4}E_3B_4/B_2+\frac{1}{4}E_2B_6'/B_1]} , \tag{D7}$$

where $B_{11}=B_3-2B_4^2/B_2-(B_6')^2/B_1$.

[1]For reviews of multicritical phenomena see, e.g., *Critical Phenomena,* Vol. 186 of *Lecture Notes in Physics,* edited by F. J. W. Hahne (Springer-Verlag, Berlin, 1983); *Multicritical Phenomena,* Vol. 106 of *NATO Advanced Studies Institute Series B: Physics,* edited by R. Pynn and A. Skjeltorp (Plenum, New York, 1983); Y. Shapira, J. Appl. Phys. **57**, 3268 (1985).

[2]M. L. Plumer and A. Caillé, paper I, Phys. Rev. B **37**, 7712 (1988).

[3]See, e.g., J. C. Tolédano and P. Tolédano, *The Landau Theory of Phase Transitions* (World Scientific, Singapore, 1987).

[4]M. L. Plumer, K. Hood, and A. Caillé, paper II, Phys. Rev. Lett. **60**, 45 (1988).

[5]W. J. L. Buyers, R. M. Morra, R. L. Armstrong, M. J. Hogan, P. Gerlach, and K. Hirakawa, Phys. Rev. Lett. **56**, 371 (1986).

[6]K. Kakurai, R. Pynn, M. Steiner, and B. Dorner, Phys. Rev. Lett. **59**, 708 (1987).

[7]P. B. Johnson, J. A. Rayne, and S. A. Friedberg, J. Appl. Phys. **50**, 1853 (1979).

[8]X. Zhu and M. B. Walker, Phys. Rev. B **34**, 8064 (1986).

[9]X. Zhu and M. B. Walker, Phys. Rev. B **36**, 3830 (1987).

[10]Similar results were obtained by B. Schaub and D. Mukamel, Phys. Rev. B **32**, 6385 (1985); D. H. Lee, R. G. Caflisch, J. D. Joannopoulos, and F. Y. Wu, *ibid.* **29**, 2680 (1984).

[11]Y. M. Gufan and V. P. Sakhnenko, Zh. Eksp. Teor. Fiz. **69**, 1428 (1975) [Sov. Phys.—JETP **42**, 728 (1975)].

[12]T. S. Chang, A. Hankey, and E. Stanely, Phys. Rev. B **8**, 346 (1973).

[13]V. J. Minkiewicz, D. E. Cox, and G. Shirane, Solid State Commun. **8**, 1001 (1970).
[14]A. Epstein, J. Makovsky, and H. Shaked, Solid State Commun. **9**, 249 (1971).
[15]Y. B. Yelon and D. E. Cox, Phys. Rev. B **6**, 204 (1972).
[16]S. J. Collocott and J. A. Rayne, J. Appl. Phys. **61**, 4404 (1987).
[17]R. Brener, E. Ehrenfreund, H. Shechter, and J. Makovsky, J. Phys. Chem. Solids **38**, 1023 (1977).
[18]K. Iio, H. Hotta, M. Sano, H. Masuda, H. Tanaka, and K. Nagata, J. Phys. Soc. Jpn. **57**, 50 (1988).
[19]K. Iio, H. Hotta, M. Sano, H. Tanaka, and K. Nagata, Tokyo Institute of Technology Technical Report No. 5746023, 1986 (unpublished).
[20]H. Kadowaki, K. Ubukoshi, K. Hirakawa, J. L. Martinez, and G. Shirane, J. Phys. Soc. Jpn. **56**, 4027 (1987).
[21]M. Habenschuss, C. Stassis, S. K. Sinha, H. W. Deckman, and F. H. Spedding, Phys. Rev. B **10**, 1020 (1974).
[22]B. D. Gaulin, M. F. Collins, and W. J. L. Buyers, J. Appl. Phys. **61**, 3409 (1987).
[23]M. O. Steinitz, M. Kahrizi, and D. A. Tindall, Phys. Rev. B **36**, 783 (1987).
[24]A. Hauser, U. Falk, P. Fischer, A. Furrer, and H. U. Güdel, J. Magn. Magn. Mater. **31-34**, 1139 (1983).
[25]R. Feile, J. K. Kjems, A. Hauser, H. U. Güdel, U. Falk, and A. Furrer, Solid State Commun. **50**, 435 (1984).
[26]H. W. Zandbergen, J. Solid State Chem. **35**, 367 (1980).